Structural Engineering and Mechanics, Vol. 8, No. 5 (1999) 491-504
DOI: http://dx.doi.org/10.12989/sem.1999.8.5.491

Gross dynamic failure of toppling block structures

James F. Wilson †

Department of Civil and Environmental Engineering, Duke University, Durham, NC 27708-0287, U.S.A.

Abstract. The initiation of toppling is explored for a uniform stack of blocks that rotates slowly about its mid-base. As the stack passes through its vertical position (θ=0), it is in free-fall rotation, and a critical inclination angle θ_c is reached at which the toppling stack "fails" or begins to crack or separate. For tall stacks (high aspect ratios), two modes of failure are hypothesized, for which the dynamic failure analyses are shown to correlate with experimental results. These block failure modes are similar to those observed for tall, toppling masonry structures with weak binding material between their brick or stone blocks.

Key words: block dynamics; block stacks; block toppling; chimney failure; masonry structures; masonry towers; structural dynamics; structural failure; tower failure.

1. Introduction

A tall, uniform masonry structure such as a brick silo or smoke stack may be thought of as a stack of blocks with a weak matrix of binding material. The dynamic stability of block stacks with rocking motion imposed at the base was addressed both theoretically and experimentally by Olsen *et al.* (1976) and by Lipscomb (1990). Equilibrium and collapse of block models for masonry structures were investigated by Como (1992) and Heyman (1992). The modeling problems associated with single blocks and block stacks under prescribed base motion or impact, with analyses of dry friction, are well documented by Sinopoli (1987, 1997), by Augusti and Sinopoli (1992), and by the many citations in the last three references. Considered herein is a related class of problems: the initiation of toppling for a uniform, solid block stack that rotates slowly about the centroidal axis at the base. As the stack passes through its vertical position (θ=0), it is in free-fall rotation, and a critical inclination angle θ_c is reached at which the toppling stack "fails" or begins to crack or separate. This study demonstrates the essential features for gross dynamic cracking of a sufficiently tall masonry structure that topples due to a weakened foundation during free-fall rotation about its mid-base.

Empirical evidence presented herein shows the existence of two and possibly three modes of dynamic failure for a toppling masonry structure and its counterpart, a stack of uniform blocks. The first mode occurs in stacks with a sufficiently high aspect ratio H, defined as the ratio of the total stack height a to the block half width b. This first mode is characterized as a lateral block separation in the form of a wedge-shaped crack at or near a point that is one-third the stack's

† Professor

height measured from the base. For instance, this first failure mode is illustrated as the larger (lower) crack in the actual chimney of Fig. 1, a chimney whose foundation was weakened during its demolition. A similar failure is also observed in a laboratory-scale toppling block stack illustrated in Fig. 2a, in which the stack has two distinct slopes, one above and one below the wedge-shaped crack. The second mode of failure is more complex, occurring only in block stacks of moderate aspect ratios. In this mode, the blocks may separate at multiple points, may show lateral slip, and may achieve free-flight while toppling. This latter failure mode is observed in the laboratory-scale toppling block stacks illustrated in Fig. 2b. A third mode of failure may also exist for block stacks of very low aspect ratios, where the coefficients of sliding friction between blocks is also small, as implied by Augusti and Sinopoli (1992). In the present investigation, this mode was observed only twice in repeated experiments. That is, shearing or relative slip was seen between adjacent blocks at the one-third point from the top of the stack, where H=3 and the observed θ_c was about 70 degrees. However, this third mode of failure requires much further work and is well beyond the scope of the present investigation.

The purposes of this investigation are to present dynamic analyses of the first two failure modes for block stacks over a wide range of aspect ratios, and to complement the theoretical results with measurements derived from laboratory-scale experiments.

Fig. 1 As this 36 m high brick chimney toppled during demolition (the base was dynamited), its first major crack appeared at about 12 m, one-third the distance up from its base. This first wedge-shaped crack is an illustration of the first gross failure mode for a high aspect ratio block structure at low angles of rotation. As the rotation proceeded, the secondary crack appeared further toward the top. (Copyrighted by Durham Herald-Sun Newspapers, Inc. and reproduced with the permission of the photographer, Harold Moore)

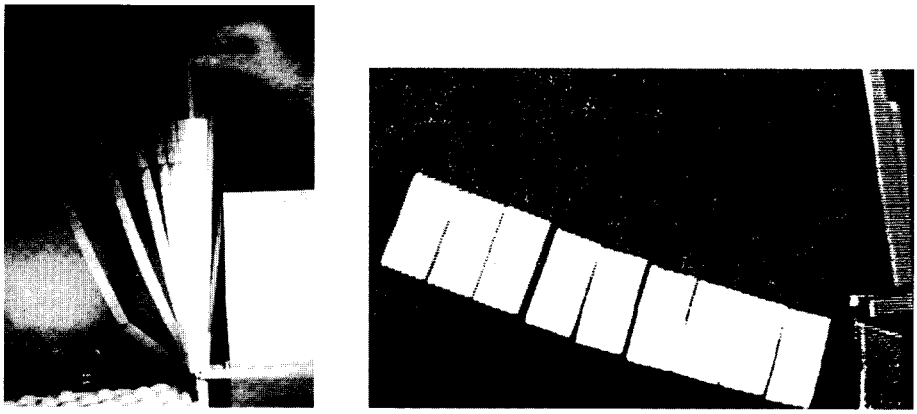

(a) (b)

Fig. 2 Typical results for the preliminary laboratory experiments for block stacks with two selected aspect ratios $H=a/b$, in which a is the block stack height and b is the block half-width. Strobe light (14 flashes/s) and one second exposure were used for photograph (a), which shows the first gross failure mode for $H=48$. Digitized video camera images were used for photograph (b), which illustrates the second gross failure mode for $H=9$

2. Analysis

An idealized model of a toppling block structure without cement between its blocks is shown in Fig. 3. This is a uniform block stack of total mass m, total height a, width $2b$, and unit depth. The stack has n identical blocks, each of height h. At time $t=0$, the initial values for the inclination angle and the angular velocity of the intact block stack are denoted by θ_0 and $\dot{\theta}_0$, respectively. Until the critical time $t=t_c$, the initial block stack acts as a rigid body that rotates in free-fall in the plane about the base point 0 with the angular acceleration $\ddot{\theta}$. At times greater than t_c, the block structure "fails"; that is, the blocks separate at different locations depending on the stack's aspect ratio, $H=a/b$. The analysis that follows lays the basis for the two gross failure modes described in subsequent sections and supported by experimental evidence.

Consider the dynamics of an intact lower segment of the block stack shown in Fig. 4. For this segment of height $y \leq a$, the mass and mass moment of inertia for plane motion about 0 are, respectively:

$$m_y = \frac{y}{a} m; \qquad I_y = \frac{1}{3} e_y m_y y^2 \tag{1}$$

in which the geometric factor e_y is defined by

$$e_y = 1 + \frac{b^2}{y^2} \tag{2}$$

Note that if the stack segment aspect ratio y/b is much larger than unity, then $e_y \approx 1$ and I_y is that of a thin rod. In general, the segment loads are: the reaction components at the pivot, R_x and R_y; the weight $m_y g$ acting at $y/2$; and V, M, and N, the shear, moment, and normal loads, respectively, acting at y. The three equations of motion for this segment rotating as a rigid body and friction-free about 0 are as follows:

$$\frac{1}{2} y m_y g \sin\theta - M - Vy = \frac{1}{3} e_y m_y y^2 \ddot{\theta} \tag{3}$$

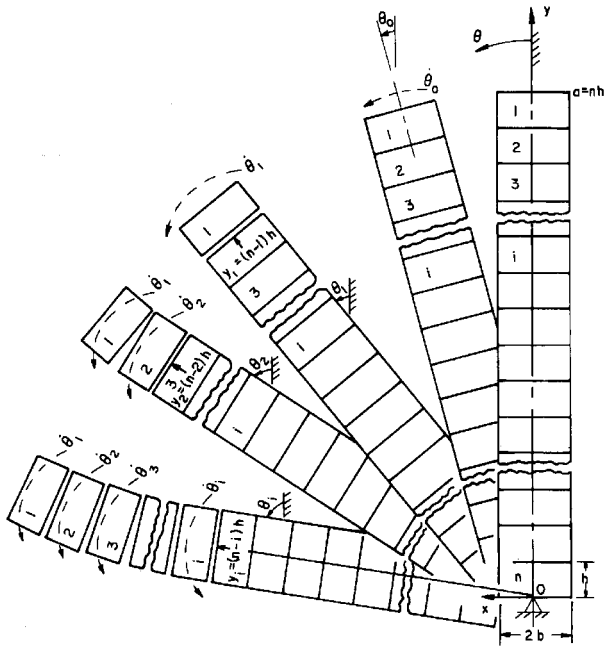

Fig. 3 Definition of block structure parameters with an illustration of the second gross failure mode for a low aspect ratio structure in which block liftoff occurs at large angles of rotation

$$m_y g \sin\theta - R_x - V = \frac{1}{2} m_y y \ddot{\theta} \tag{4}$$

$$R_y - N - m_y g \cos\theta = -\frac{1}{2} m_y \dot{\theta}^2 y \tag{5}$$

Consider now the motion of the full, intact block stack for which $y=a$, $m_y=m$, and $e_y=e=1+b^2/a^2$. At the top of the stack ($y=a$) the surface is traction-free, or $V=M=N=0$. These conditions are used to compute $\ddot{\theta}$ and R_x from Eqs. (3) and (4), or

$$\ddot{\theta} = \frac{3g}{2ea} \sin\theta \tag{6}$$

$$R_x = (1 - \frac{3}{4e}) mg \sin\theta \tag{7}$$

It is emphasized that the block stack's internal loads M, V, N depend on the inertia forces and can be expressed as functions of θ only if Eq. (6) is valid, which is for a rigid body block stack in motion in the range $0 \leq \theta \leq \theta_c$.

The state (θ, $\dot{\theta}$) of the full stack is related to the stack's initial state (θ_0, $\dot{\theta}_0$) through the conservation of energy equation in which the sum of the kinetic and potential energies remains constant. This equation is

$$\frac{1}{2}\left(\frac{e}{3} ma^2\right)(\dot{\theta}^2 - \dot{\theta}_0^2) = \frac{1}{2} mga(\cos\theta_0 - \cos\theta) \tag{8}$$

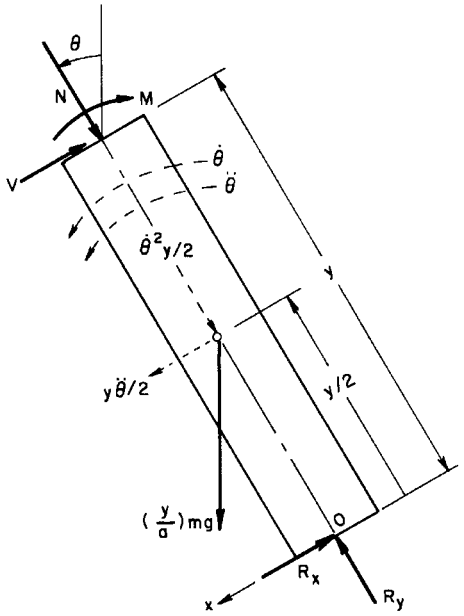

Fig. 4 Definition of system parameters for an intact lower segment of a block stack of height y

With the traction-free conditions above and with $\dot{\theta}$ from this energy relationship, R_y is computed from Eq. (5), or

$$R_y = mg\left[\left(1+\frac{3}{2e}\right)\cos\theta - \frac{3}{2e}\cos\theta_0 - \frac{a}{2g}\dot{\theta}_0^2\right] \tag{9}$$

The explicit results for $\ddot{\theta}$, R_x, $\dot{\theta}^2$, and R_y given by Eqs. (6)-(9) are sufficient for computing the internal loads V, M, and N from Eqs. (3)-(5) in terms of nondimensional system parameters and initial conditions. The nondimensional system parameters are:

$$e = 1+\frac{1}{H^2}, \quad H = \frac{a}{b}, \quad Y = \frac{y}{a}, \quad \Omega_0^2 = \frac{\dot{\theta}_0^2 h}{g} \tag{10}$$

$$\bar{V} = \frac{V}{mg}, \quad \bar{M} = \frac{M}{mga}, \quad \bar{N} = \frac{N}{mg} \tag{11}$$

With Eqs. (6)-(11), Eqs. (3)-(5) lead to the following results.

$$\bar{V} = -\frac{1}{4e}(3Y^2 - 4eY + 4e - 3)\sin\theta \tag{12}$$

$$\bar{M} = \frac{1}{4e}Y(Y^2 - 2eY + 2e - 1)\sin\theta \tag{13}$$

$$\bar{N} = \frac{1}{2e}(1-Y)[(3Y + 2e + 3)\cos\theta - 3(Y+1)\cos\theta_0 - eA\,\Omega_0^2(1+Y)] \tag{14}$$

Plots of these three internal loads given by Eqs. (12)-(14) are shown in Figs. 5-7, respectively. These results are for cases where $b^2/a^2 \ll 1$ (or e=1) and for free-fall in rotation which begins with

the initial conditions of $\theta=\theta_0=0$ and $0<\Omega_0\ll 1$ at time zero. (This free-fall in rotation is modeled after the experimental apparatus shown in Fig. 9 and discussed in the Experimental Methods section). The three main features of the three internal loads as a function of Y and θ illustrated in these figures are summarized. First, the respective critical locations $Y=Y_c$ of the extrema for $\bar{V}$ and $\bar{M}$, computed by setting $d\bar{V}/dY=0$ and $d\bar{M}/dY=0$, are:

$$Y_c = \frac{2e}{3} \qquad \text{(extremum: } \bar{V}\text{)} \tag{15}$$

$$Y_c = \frac{2e}{3} - \frac{1}{3}(4e^2 - 6e + 3)^{1/2} \qquad \text{(extremum: } \bar{M}\text{)} \tag{16}$$

In the special case of high aspect ratios H (or $b^2/a^2\ll 1$ and $e=1$), the respective extrema for $\bar{V}$ and $\bar{M}$ occur at values of $Y=Y_c$ of 2/3 and 1/3, at which the corresponding peak shear and moment loads are $(\sin\theta)/12$ and $(\sin\theta)/27$. Second, $\bar{N}$, which must be positive to insure compressive loading at the block interfaces, is a maximum at $Y=0$. This is seen in Fig. 7. Third, when one follows the $\theta=40$ deg curve in Fig. 7, it is noted that $\bar{N}$ is always positive (a compressive load). By observing this and the other curves, one may imagine a critical curve for which θ just exceeds 40 deg, for which a positive $\bar{N}$ approaches zero, and for which the slope approaches zero at $\bar{Y}=1$. Thus, it is seen that a lower bound on the inclination angle $\theta=\theta_c$ at which $\bar{N}$ passes through zero from positive to negative, may be found by computing $d\bar{N}/dY=0$ and setting $Y=1$. The result is:

$$\theta_c = \cos^{-1}\left[\frac{3\cos\theta_0 + \Omega_0^2 Ae}{3+e}\right] \tag{17}$$

For the those cases where $\theta_0=0$, $\Omega_0^2\ll 1$, and $e=1$, then $\theta_c=\cos^{-1}(3/4)=41.41$deg. This lower bound angle at which the top block just separates from the intact stack below, is never realized. This is because the blocks are of finite height and of finite number n. Thus, separation first occurs not at $Y=1$ but at $Y=(n-1)/n$, at an angle somewhat larger than 41.41 deg.

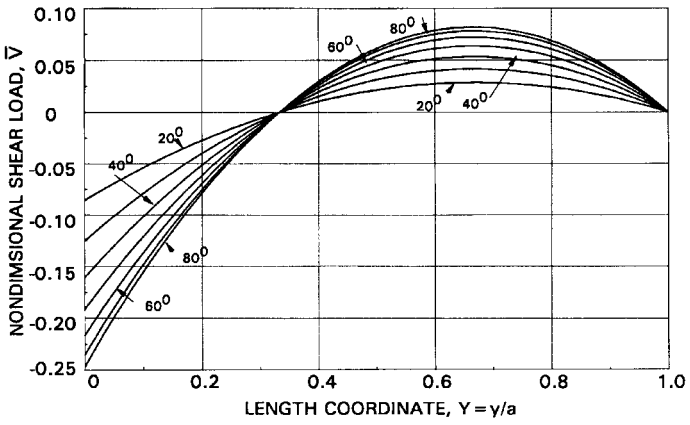

Fig. 5 Shear load distribution along the length of an intact block stack at various angles of rotation. Initially, $\theta_0=0$ and $\dot{\theta}_0\simeq 0$. Results are for $H\gg 1$ and $e=1$

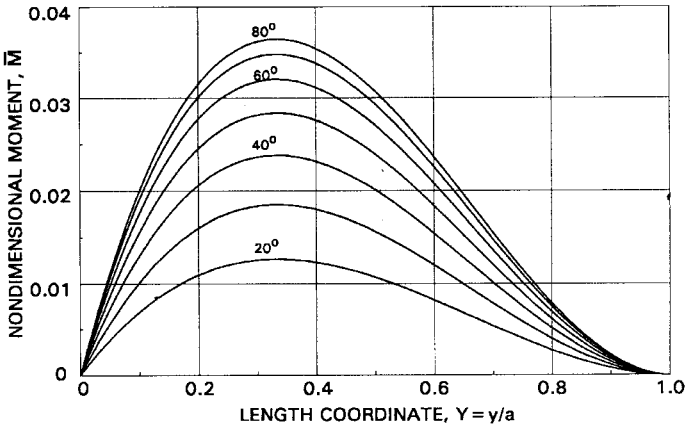

Fig. 6 Moment distribution along the length of an intact block stack at various angles of rotation. Initially, $\theta_0=0$ and $\dot{\theta}_0\approx 0$. Results are for $H\gg 1$ and $e=1$

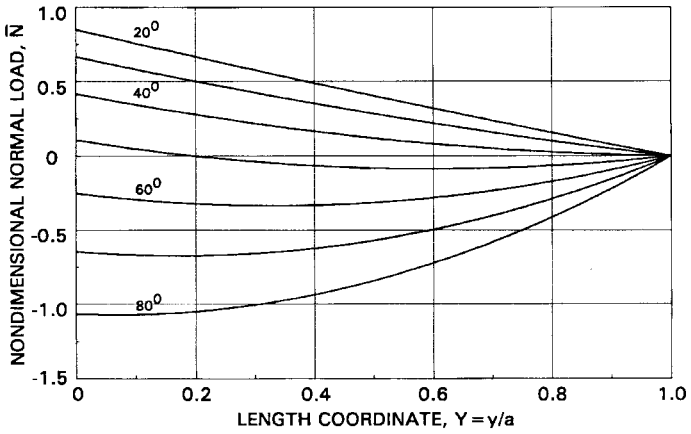

Fig. 7 Normal load distribution along the length of an intact block stack at various angles of rotation. Initially, $\theta_0=0$ and $\dot{\theta}_0\approx 0$. These results are applicable to non-cemented block stacks in which $\bar{N}\geq 0$, $\theta<41.41$ deg, $H\gg 1$, and $e=1$

3. Two dominant mechanisms for gross failure

The predicted behavior of $\bar{M}$ and $\bar{N}$, together with the physical evidence presented in Figs. 1 and 2, suggest that there are two dominant modes of gross failure of a block stack in free-fall rotation. The first mode occurs for stacks with high aspect ratios, for $H>18$, for $\theta<41.41$ deg, and is observed as a wedge-shaped crack at or near $Y=1/3$, the point of the peak internal moment $\bar{M}$. This first (and largest) crack is observed in toppling brick chimney of Fig. 1 and in the laboratory stack of Fig. 2a. The second mode occurs on stacks with $H<18$, for $\theta>41.41$ deg, and appears as each block, starting with the top one, lifts off one by one from the intact stack below it. This second mode is observed in the photograph of Fig. 2b.

The criterion for the first mode of gross failure is hypothesized in the form $fM-bN=0$. Here, f is defined as the moment deficit factor, a constant that is derived from experiment. That is, M and N are computed from the analysis at the point y of the first observed crack, from which the

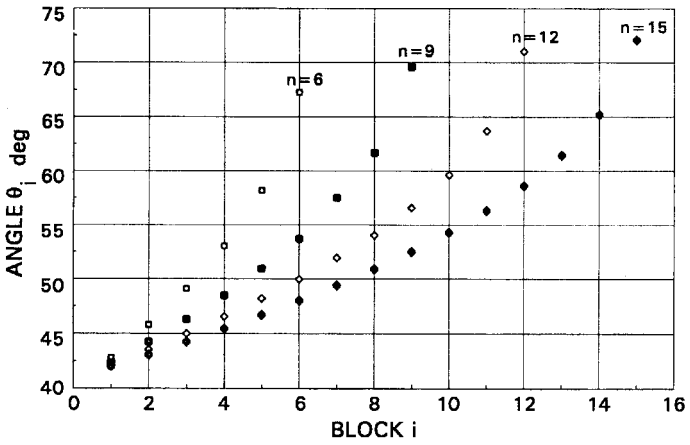

Fig. 8 Theoretical results for the second gross failure mode. For each of the four block stacks $H=n=6$, 9, 12, and 16, the critical liftoff angle θ_i is shown for each block i of the stack

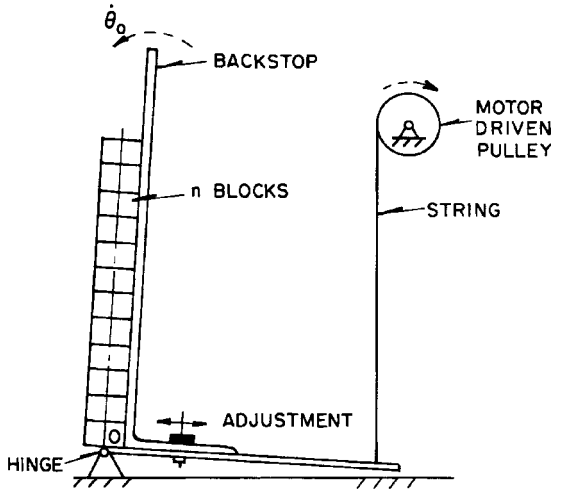

Fig. 9 The laboratory-scale experimental system. The aluminum backstop, driven by the motor, has an angular velocity of $\dot{\theta}_0$=0.0393 rad/s. The respective length, width, and height dimensions of each steel block are 2.54 cm, 2.54 cm, and 1.47 cm

measure $f=bN/M$ is then obtained. Just prior to forming a wedge-shaped crack such as the one on the lower left in Fig. 1, the dynamic moment fM is balanced by the equivalent dynamic moment bN about the right edge of the impending crack. During free-fall rotation of a "no tension" block stack, at the point of impending cracking, M is increasing as the neutral axis in bending moves toward the compression edge. By this hypothesis, complete separation occurs when $M=bN$, or for $f=1$. In practice, f is measured to be less than unity, which implies that the toppling blocks do sustain some tension, as will be discussed presently. Using the nondimensional parameters of Eqs. (10) and (11), the criterion for the first mode of gross failure that includes the moment deficit is thus:

$$Hf\bar{M} - \bar{N} = 0 \tag{18}$$

The criterion for the second mode of gross failure is the liftoff mode defined in Fig. 3, hypothesized for rotations θ greater than 41.41 deg. Liftoff is expressed by two recursion relationships which are derived as follows. At $a=nh$, both θ_0 and $\dot{\theta}_0$ are given. Then as the initially intact block stack ($a=a_1=nh$) reaches the critical angle $\theta=\theta_1$, the normal load N at $y=y_1=(n-1)h$, the interface of blocks 1 and 2, approaches zero and liftoff of block 1 is imminent. In general, the length a_i of the intact block stack that rotates from θ_{i-1} to θ_i, where liftoff of block i is imminent, is $a=a_i=y_i+h=(n-i+1)h$; and this location is also expressed as $Y=Y_i=y_i/a_i=(n-i)/(n-i+1)$. In addition, $e=e_i=1+b^2/a_i^2$. These subscripted parameters then replace their non-subscripted counterparts in Eq. (14) where $\bar{N}=0$; and the subscript $i-1$ denoting the initial state replaces the subscript ($_0$) denoting the general initial state. Thus, the first recursion formula is obtained as:

$$\cos\theta_i = [3\cos\theta_{i-1} + P(i,n,B)\,\Omega_{i-1}^2]\,Q(i,n,B) \tag{19}$$

in which $i=1, 2, \ldots, n$ and

$$P(i,n,B) = \frac{(n-i+1)^2+B^2}{(n-i+1)} \tag{20}$$

$$Q(i,n,B) = \frac{(2n-2i+1)(n-i+1)}{(n-i+1)(8n-8i+5)+2B^2} \tag{21}$$

The second recursion formula is based on the energy Eq. (8) and relates the angular velocity of the intact stack at state i to that at state $i-1$. With the nondimensional forms of Eqs. (10) and (11), Eq. (8) is rewritten to obtain the second recursion formula for the second gross failure mode, or

$$\Omega_i^2 = \Omega_{i-1}^2 + \frac{3(n-i+1)}{(n-i+1)^2+B^2}(\cos\theta_{i-1} - \cos\theta_i) \tag{22}$$

Thus, given (b, h, n) and the initial state (θ_0, $\dot{\theta}_0$), and with Ω_0^2 computed from Eq. (10), consecutive sets of solutions (θ_i, Ω_i) may be computed from Eqs. (19)-(22) for $i=1, 2 \ldots, n$. For instance, for each block i in a given stack of n blocks ($n=6, 9, 12, 15$), the initial lift off angle θ_i was calculated in this way. These results are shown in Fig. 8. It should be kept in mind that the basic assumption of this model characterizing the second mode of gross failure is that once a block achieves free flight, it no longer comes in contact with its nearest neighbor.

4. Experimental method

To design the final experiments to accurately measure the onset of the first two hypothesized modes of failure, three types of simple preliminary experiments were performed. These three experiments, described in detail by Wilson (1993a), are now summarized. The first of these preliminary experiments employed standard, solid red building bricks, uniformly stacked lengthwise (end-to-end), with one face resting against a nearly vertical backstop, a wood plank. The brick stack rested on a small shelf of width b, the half the thickness of a brick. This shelf, attached to the bottom of the backstop, rested on a base pivot. To hold the stack together during the initial stage of the free fall, the sticky side of a nylon-reinforced binding tape ("duct" tape) was applied on the opposite sides of the brick faces, along the whole length of the stack. Such tape was used only in this particular set of full-sized building brick experiments. In repeatable

tests, the backstop-block stack assembly (similar to that shown in Fig. 9) was slowly tipped by hand through its vertical position, the stack toppled intact as it rotated about its mid-base pivot through about a 45 deg angle, and then the binding tape on the outer face broke at the third point from its base. This same result was observed for uniform brick stacks of several different aspect ratios, for $H \geq 18$, in which the stacked number of bricks was always an integer multiple of three. These first series of preliminary experiments clearly demonstrated the existence of the first failure mode; but the second failure mode was not observed for $H \leq 15$ because the binding tape across the brick faces supressed any tendency for blocks to separate in that mode.

The second set of preliminary experiments were laboratory-scale and employed the fixture shown in Fig. 9. In the beginning, the backstop was not motor-driven, but slowly pushed through the vertical position by hand. Solid, smooth steel blocks carefully machined to the following dimensions were used: $1.27 \times 2.54 \times 2.54$ cm. Each experiment was performed for these blocks stacked in multiples of three and for aspect ratios $H=a/b$ ranging from 6 to 48. Strobe light photography was used to observe the modes of failure, with light flashes of 14 per second and with the camera shutter open for about one second, the approximate time for the tallest stacks to topple. A typical result is shown in Fig. 2a in which the first failure mode, cracking at the third point, was observed for $H=48$.

The third set of preliminary experiments were the same as the second set, but without the strobe light. Toppling was recorded with an analog video camera with a digitizing image system. At 30 frames per second, this system gave large, reasonably clear individual images. A typical result is shown in Fig. 2b in which the second failure mode, or multiple separations along the length, was observed for $H=9$.

The preliminary experiments illustrated the two failure modes and also indicated the need for higher frame rates to accurately measure the inclination angles and locations along the stack at the first appearance of a crack. Thus, in the final experiments 100 frames per second were photographed using a Fairchild high speed 16 mm motion analysis camera, model HS401. In these final experiments, the same laboratory-scale blocks described above were used, together with the motor-driven system shown in Fig. 9 for initiating toppling. From two to four experiments were performed for each of the following aspect ratios: $H=a/b=n=6$, 9, 12, 15, 18, 21, and 24. In the final 21 experiments, the backstop with its carefully aligned blocks was slowly driven toward its vertical position by the motor so that at its initial state, $\theta=\theta_0=0$, the angular velocity of the stack was a constant $\dot{\theta}_0=0.0393$ rad/s or $\Omega_0=0.00489$. Each of the approximately 100 images for each of the 21 experiments was then examined to determine the onset of failure. For each experiment, the following data were gleaned from these images: the lowest inclination angle $\theta=\theta_c$ and the location $Y=Y_c$ for the first appearance of a wedge-shaped crack (mode one failure); or $\theta=\theta_i$ corresponding to the first appearance of approximate parallel separation between adjacent blocks (mode two failure). These critical data for the 21 experiments are listed in Tables 1 and 2, which are evaluated and compared to theory in the next section.

5. Experimental results and discussion

To test the validity of the first mode of gross failure, the experimental results of Table 1 were correlated with the failure theory of Eq. (18) as follows. First, considering the twelve data sets (H, Y_c, θ_c), the set (18, 0.222, 42.5) was deleted since θ_c exceeded the threshhold angle of 41.41 deg required to maintain compressive loading between blocks. For each of the remaining eleven data

sets, the corresponding pair ($\bar{N}$, $H\bar{M}$) was computed from Eqs. (13) and (14) in which $Y=Y_c$, $\theta=\theta_c$, $\theta_0=0$, $\Omega_0=0.00489$ and $e=1$. For each computed pair ($\bar{N}$, $H\bar{M}$), the moment deficit factor f was computed from Eq. (18). With those values of f, listed in Table 1, and the statistical package PSI-Plot (1994), the arithmetic mean, the standard deviation, and the 95% confidence interval for f were calculated. Chauvenet's Criterion was then applied, with the result that the data set ($H=21$, $Y_c=0.143$, $\theta_c=29.5$) was spurious (outside a normal distribution) and thus could be eliminated from the data set of eleven. See Wilson (1993b). The data and the statistical results for Y_c, θ_c and f based on the remaining ten data sets are given in Table 1.

The four main experimental results for the data of Table 1, the first gross failure mode, are summarized: (1) This mode dominates for aspect ratios of $H \geq 18$; (2) This mode occurs at a mean measured nondimensional distance of $Y_c=0.329$ (or at approximately one-third the height of the stack from the base pivot point). The standard deviation of Y_c is 0.08 and the 95% confidence interval is 0.272 to 0.386; (3) This mode occurs at a mean measured angle of inclination of θ_c of 34.5 deg, where the standard deviation is 2.96 deg and the 95% confidence interval is 32.4 deg to 36.6 deg. These measures are well within the predicted theoretical threshhold value of 41.41 deg; (4) This mode leads to a moment deficit factor of $f=0.746$ (or approximately 3/4), where the standard deviation of f is 0.166 and the 95% confidence interval is 0.628 to 0.865.

This last result for f warrants further consideration. In the discussion just preceding Eq. (18) of the hypothesized criterion for the first failure mode, $fM=bN$, a no-tension block stack in free-fall rotation has a minimum moment deficit factor of $f=1$. Except for Test 12 of Table 1 in which

Table 1. Listed are the experimental data for 12 tests that showed the first gross failure mode. Measures of imminent failure are the critical inclination angles θ_c their corresponding locations Y_c. The moment deficit factor f was computed from these data using Eq. (18)

Test No.	$H=n$	Y_c	θ_c deg	f
1	24	0.417	33.5	0.597
2	24	0.417	30.5	0.786
3	24	0.375	32.5	0.689
4	24	0.375	33.0	0.661
5	21	0.190	35.0	0.977
6	21	0.143	29.5	—
7	21	0.286	32.0	0.799
8	21	0.286	34.5	0.557
9	18	0.222	42.5	—
10	18	0.389	37.5	0.692
11	18	0.333	36.5	0.637
12	18	0.222	40.5	1.072
	arithmetic mean	0.329	34.5	0.746
	standard deviation	0.080	2.96	0.166
	95% confidence interval	0.272 to 0.386	32.4 to 36.6	0.628 to 0.865

Table 2. Listed are the experimental data for fourteen tests that showed the second gross failure modes. The measured lowest inclination angles θ_i are for blocks i below which gross block separations were first observed. The % deviation= $100(\theta_i$ theoretical $- \theta_i$ experimental$)/\theta_i$ theoretical

Test No.	$H=n$	i	θ_i deg experimental	θ_i deg theoretical	% deviation
13	15	5	49.5	46.78	-5.81
	15	10	49.5	54.47	9.12
14	15	7	43.0	49.51	13.1
	15	11	43.0	56.51	23.9
15	15	8	50.5	51.02	1.0
	15	11	50.5	56.51	10.6
16	12	8	65.5	54.33	-20.6
17	12	8	60.5	54.33	-11.4
18	9	4	73.0	48.74	-49.8
	9	6	73.0	54.13	-34.9
19	9	5	67.0	51.24	-30.8
	9	6	67.0	54.13	-23.8
20	6	3	65.0	49.69	-30.8
21	6	3	65.0	49.69	-30.8

f=1.072, the values of f are less than unity. In such cases, it follows that $M/N=b/f>b$, which implies that the resultant of the tractions M and N is physically outside the block width as cracking begins. Since such a scenario is not possible, then some combination of tensile and compression loads (with a resultant net compressive load of N) must exist between the block faces just prior to cracking. In these experiments, unlike those preliminary experiments involving stacks of actual building bricks, no binding tape was used to hold the blocks together, leading to tensile loads. However, there may be three minor factors that could possibly lead to tensile loads: (1) slight deformations of the steel blocks that before failure would reduce the inertia forces and thus reduce M (this would stretch the imagination); (2) imperfections in block geometry; and (3) initial eccentric stacking of the blocks. Most likely, the small tensile loads that lead to the low values of f were due to natural adhesion between the block contact surfaces, which were machined as smooth as possible and covered with a thin coat of oil to prevent corrosion. Further, the effects of friction between blocks was not accounted for in the theory or failure hypothesis.

The experimental data for the second mode of gross failure, or block separations with liftoff that typify the lower range of aspect ratios, are summarized in Table 2. The test numbers 13 to 21 represent nine separate experiments. In each of the tests 13, 14, 15, 18, and 19, there were two points on the stack where block separation was observed; but for the other four tests, there was only one block separation each. In Table 2, the critical block i is that block below which separation was first observed, and for which the corresponding angle is θ_i. (Recall that the blocks are numbered starting at the top of the stack).

Consider the results of Table 2. For H=15, most of the data shows that theory overestimates by about 1% to 24% the measured critical angles θ_i for impending block separation. For H values of 12, 9, and 6, however, the theory underestimates the measured values of θ_i by about 11% to 50%. Overall, the mean value for the percent deviation of measurement from the theory is -12.9%, with a 95% confidence interval of -25.6% to -0.2%. Acccording to the theoretical model, one would expect to observe sequential separations beginning at the top block. Such was not observed for either or both of the following two reasons. First, the block separations at threshhold levels were just too small to be resolved from the film images; and second, adhesion of the smooth steel block interfaces required an extra tensile load normal to the surfaces for separation to occur; but adhesion was not accounted for in the theoretical model. Thus, impending gross failure could be observed only at larger than predicted inclination angles. In future investigations, the mean deviation of -12.9% of measurement compared to theory could be improved by improving photographic image resolution and including in the theory the effects of both block adhesion and sliding friction at the block interfaces.

6. Conclusions

It was found that the experimental data correlated well with a moment deficit hypothesis characterizing the first mode of gross failure, and that the experiments provided some results that the theory could not. Experiments showed that for aspect ratios $H \geq 18$, this first mode was dominant; that a wedge crack first appeared at a mean distance of Y_c=0.329 from the base (theory predicted Y_c=1/3); and that this failure occurred at a mean inclination angle of θ_c=34.5 deg. The latter result was consistent with theory which predicted inclination angles for impending mode one failure could not exceed 41.41 deg. Further, the mean value for the moment deficit factor f, a possible physical constant for toppling block stacks, was measured as f=0.742 (standard deviation= 0.166). The fact that f was less than unity, the value predicted for zero tension at the block faces, implied that some adhesion did exist between the experimental block faces.

While the above results were valid for $H \geq 18$, the second mode of gross failure (liftoff), was observed for lower aspect ratios: $H \leq 15$. The measured angles for block liftoff (impending parallel block separation), were always above the threshhold inclination angle of 41.41 deg at which theory predicted full loss of compressive load between the topmost adjacent blocks. However, compared to the liftoff theory, presented as two recursion formulas depicting consecutive block liftoff from the top block and downward, the measured values of the inclination angles θ_i for blocks i were generally higher for H=15 and lower for lower aspect ratios. Overall, the mean deviation of these measured angles from theory was -12.9%. A better agreement between theory and experiment in this mode of failure could probably be achieved in three ways: by improving the experiments to minimize adhesion between adjacent blocks, which delayed liftoff; by incorporating block adhesion in the theory; and by improving the resolution of the high speed photography. Nevertheless, the present exploratory studies on toppling blocks provide some new insights about the gross failure modes of toppling masonry structures. Future investigations may involve a third mode of failure for the free-fall rotations of block stacks of low aspect ratios ($H \leq$ 6) in which sliding friction between blocks is incorporated in the theory.

Acknowledgments

The author is grateful to Ina Inesa, Carmen Stubig, and Martin Trively who patiently assisted with the experiments; to Nayer El-Esnawy who aided in the analysis and computations; and to the reviewers who kept me honest and suggested the third mode of failure.

References

Agusti, G. and Simopoli, A. (1992), "Modelling the dynamics of large block structures", *Meccanica,* **27**(3), 195-211.

Como, M. (1992), "Equilibrium and collapse of masonry bodies", *Meccanica,* **27**(3), 185-194.

Heyman, J. (1992), "Leaning towers", *Meccanica,* **27**(3), 153-159.

Lipscombe, P.R. (1990), "Dynamics of rigid block structures", PhD Thesis, University of Cambridge, Cambridge, England.

Olsen, B.E., Neylan, A.J. and Gorholt, W. (1976), "Seismic test on a one-fifth scale HTGR core model", *Nuclear Engineering Design,* **36**.

PSI-Plot, (1994), *Technical Plotting and Data Processing, Version 3*, Polyscience International, Salt Lake City, UT.

Sinopoli, A. (1987), "Dynamics and impact in a system with unilateral constraints: The relevance of dry friction", *Meccanica,* **22**(4), 210-215.

Sinopoli, A. (1997), "Unilaterality and dry friction: A geometric formulation for two-dimensional rigid body dynamics", *Nonlinear Dynamics,* **12**, 343-366.

Wilson, J.F. (1993a), *Experiments on the Dynamics of Solids*, Experiment 19: "Cracking of a toppling chimney", McGraw-Hill, College Custom Series, N.Y.

Wilson, J.F. (1993b), *Experimental Solid Mechanics*, Chapter 2, McGraw-Hill, College Custom Series, N.Y.